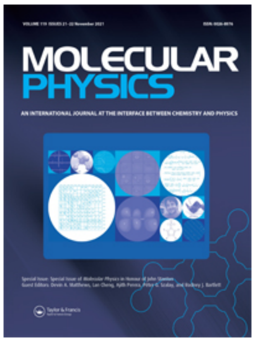

Taylor & Francis
Taylor & Francis Group

Molecular Physics
An International Journal at the Interface Between Chemistry and Physics

ISSN: (Print) (Online) Journal homepage: https://www.tandfonline.com/loi/tmph20

The 130–360 GHz rotational spectrum of *syn*-2-cyano-1,3-butadiene (C_5H_5N) – a molecule of astrochemical relevance

Maria A. Zdanovskaia, Brian J. Esselman, Samuel M. Kougias, Aatmik R. Patel, R. Claude Woods & Robert J. McMahon

MOLECULAR PHYSICS
2021, VOL. 119, NOS. 21–22, e1964629 (14 pages)
https://doi.org/10.1080/00268976.2021.1964629

Taylor & Francis
Taylor & Francis Group

JOHN STANTON SPECIAL ISSUE: THEORY MEETS EXPERIMENT

The 130–360 GHz rotational spectrum of *syn*-2-cyano-1,3-butadiene (C_5H_5N) – a molecule of astrochemical relevance

Maria A. Zdanovskaia, Brian J. Esselman, Samuel M. Kougias, Aatmik R. Patel, R. Claude Woods and Robert J. McMahon

Department of Chemistry, University of Wisconsin–Madison, Madison, WI, USA

ABSTRACT

The analysis of *syn*-2-cyano-1,3-butadiene (C_5H_5N, $\mu_a = 3.2$ D, $\mu_b = 2.3$ D) in its ground vibrational state and two lowest-energy excited vibrational states, ν_{27} (A″, 144 cm^{-1}) and ν_{19} (A′, 163 cm^{-1}), in the 130–360 GHz frequency region has been completed. Nearly 4200 rotational transitions have been measured in the ground vibrational state for the first time, resulting in the determination of the spectroscopic constants for a complete octic Hamiltonian with low error. Analysis of the two lowest-energy, Coriolis-coupled fundamentals reported herein, each containing circa 3000 transitions, yielded two possible least-squares fitting solutions. Both solutions address perturbation between the two vibrational states, including resonances and several nominal interstate transitions, using four *a*-type and five *b*-type Coriolis coupling terms (G_a, G_a^J, G_a^K, F_{bc}, G_b, G_b^K, F_{ac}, and F_{ac}^K, with or without F_{ac}^J). The energy separation between the two states, $\Delta E_{27,19} = 12.307065$ (2) cm^{-1}, agrees between the two solutions within their statistical uncertainties, giving confidence that this value is accurate despite the differing Coriolis-coupling terms. The precise rotational and distortion constants determined in this work provide the foundation for an astronomical search for *syn*-2-cyano-1,3-butadiene across the radio band.

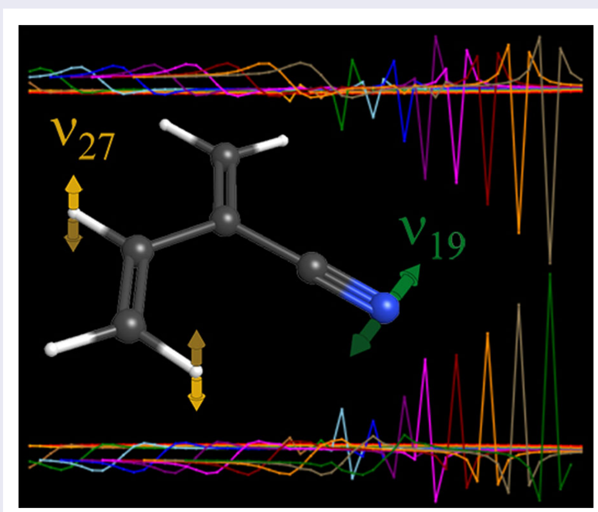

ARTICLE HISTORY
Received 29 May 2021
Accepted 29 July 2021

KEYWORDS
Astrochemistry; Coriolis coupling; rotational spectroscopy; pyridine isomer; Titan atmosphere

Introduction

More than 200 molecules have been detected in the interstellar medium (ISM) or in circumstellar shells – the majority of these detections *via* radioastronomy [1,2]. Approximately ten percent of the detected species are organic nitriles, including recent detections of benzonitrile [3], 1- and 2-cyanonaphthalene [4], hydroxyacetonitrile [5], and silyl cyanide [6]. Due to their characteristically strong dipole moments and composition of relatively abundant elements, nitriles (R–CN) represent

CONTACT Robert J. McMahon robert.mcmahon@wisc.edu Department of Chemistry, University of Wisconsin–Madison, Madison, WI 53706, USA

Supplemental data for this article can be accessed here https://doi.org/10.1080/00268976.2021.1964629

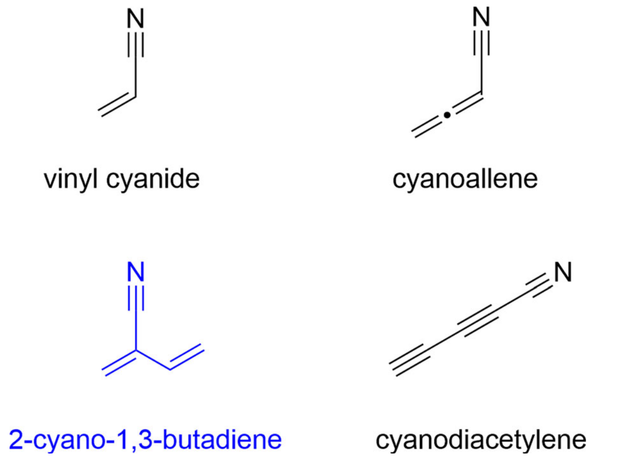

Figure 1. Nitriles detected in the ISM (vinyl cyanide, cyanoallene, and cyanodiacetylene) with structures similar to 2-cyano-1,3-butadiene.

inviting targets for additional radioastronomical detections. A series of highly unsaturated nitrile-containing carbon chains ($HC_{2n+1}N$ with $n = 0$–5) have been detected [7–12], as well as several partially unsaturated [13–16] and fully saturated [17–19] organic nitriles. Specifically, the known interstellar molecules vinyl cyanide (C_3H_3N) [14], cyanoallene (C_4H_3N) [16], and cyanodiacetylene (C_5HN) [7] exhibit structural similarities to the molecule of interest in the current work: 2-cyano-1,3-butadiene (C_5H_5N) (Figure 1). Our group synthesised and characterised several astrochemically relevant nitriles and isonitriles in order to analyse their rotational spectra [20–23]. Although neither McCarthy *et al.*, who examined the electrical discharge of benzene with molecular nitrogen [24], nor Zwier and coauthors, who examined the gas-phase pyrolysis of 3-pentenenitrile [25], detected 2-cyano-1,3-butadiene among their products, it may nevertheless be considered a likely interstellar molecule. Irradiation of cyanoacetylene with ethylene with 254 nm light, for example, produces 2-cyano-1,3-butadiene [26]. A theoretical study suggested that 2-cyano-1,3-butadiene is a predominant product in the reactions of cyano radical with 1,2-butadiene and cyano radical with 1-butyne [27]. There are, however, no published spectroscopic data available to enable a radioastronomical search for this nitrile.

An additional reason for targeting the cyano-butadiene isomers is that they share the same molecular formula as pyridine (C_5H_5N, $\mu = 2.19$ D). Pyridine, along with several other nitrogen heterocycles, is an aromatic molecule of substantial astrochemical interest. Not only has pyridine been implicated as a building block for nitrogen-substituted polycyclic aromatic hydrocarbons (NPAHs) [28], but it is also a building block of nicotinic acid (Vitamin B3) and nicotinamide. These pyridine-based moieties are precursors to nicotinamide adenine dinucleotide (NAD), a key coenzyme in metabolism [29]. Nicotinic acid of interstellar origin has been detected on the Murchison meteorite [30,31], and a possible route to interstellar formation from pyridine has also been suggested [32]. Detection of extraterrestrial pyridine could shed light on the chemistry occurring in extreme, prebiotic environments. To date, however, pyridine has eluded detection in the ISM [33]. This work on 2-cyano-1,3-butadiene could enable its detection in the ISM and an exploration of the chemistry of C_5H_5N species in that environment.

Materials and methods

Experimental

As described recently, 2-cyano-1,3-butadiene was prepared from acrylonitrile and acetaldehyde and purified by distillation [22]. Rotational spectra were collected on a broadband spectrometer with a pressure of 3 mTorr at room temperature. The 130–360 GHz spectrum was collected using the instrument described previously [21,34], using two separate Virginia Diodes amplification and multiplication chains and Virginia Diodes Zero-Bias Detectors for the 130–230 GHz and 235–360 GHz frequency segments. In each region of the spectrum, we assume a uniform frequency measurement uncertainty of 0.05 MHz. The spectra were combined into a single broadband spectrum using Assignment and Analysis of Broadband Spectra (AABS) software [35,36]. Pickett's SPFIT and SPCAT programs [37] were used to conduct least-squares fitting and spectral prediction, respectively. Kisiel's PIFORM, PMIXC, PLANM, and AC programs were used to analyse data, reformat output files, and generate various plots [38].

Computational

Density functional theory computations were performed at the B3LYP/6-311+G(2d,p) level of theory using Gaussian 16 software [39] and the WebMO [40] user interface. Optimised geometries for *syn*- and *gauche*-2-cyano-1,3-butadiene were obtained using 'very tight' convergence criteria and an 'ultrafine' integration grid (opt = verytight int = grid = ultrafine). Anharmonic vibrational frequency calculations provided the fundamental vibrations, the vibration-rotation interaction constants (A_0–A_v), and the Coriolis coupling (ζ) constants. A relaxed coordinate scan of rotation about the central C–C bond for 2-cyano-1,3-butadiene was also performed. An optimisation and anharmonic vibrational frequency calculation using the above-described criteria were also performed for the *syn-syn-cis* (SSC) conformer of glycolic acid [41] to enable direct comparison of computational accuracies. Computational output files are provided in the supplemental material.

Results

Conformational analysis of 2-cyano-1,3-butadiene

Like 1,3-butadiene [42], 2-cyano-1,3-butadiene has two low-energy conformations – *syn* and *gauche*. The *syn* conformation is a planar, C_s structure that allows effective π conjugation throughout the molecule. The higher-energy *gauche* conformations are an enantiomeric pair of nonplanar, C_1 structures, in which steric interactions between the methylene groups create a twist around the central C–C bond. The computed dihedral angle between the two terminal carbon atoms of *gauche*-2-cyano-1,3-butadiene is 33.3°, a value similar to that determined for 1,3-butadiene (33.8 (13)°) [42]. The computed energy difference between the *syn* and *gauche* conformers is 3.1 kcal/mol or 1080 cm^{-1} (including ZPVE). The barrier to conformational exchange (Figure 2) is only 6.5 kcal/mol, which allows these species to interconvert readily at room temperature. Even if assuming the statistical doubling due to two enantiomeric forms of the *gauche* conformer, the energy difference of ca. 3 kcal/mol results in an equilibrium population of the *gauche* conformational isomer of only 1.0% of the total for 2-cyano-1,3-butadiene at the temperature the spectrum was collected (298 K). This low population makes the detection of the *gauche* conformation unlikely, due to the high spectral density of the *syn* conformation. Detection of the *gauche* conformer is further complicated by its possible tunnelling splitting, which would nullify the statistical doubling in intensity and make the distorted rotor prediction insufficient to assign its transitions. The *syn* conformer of 2-cyano-1,3-butadiene is only about 1 kcal/mol higher in energy than the *E*-1-cyano isomer, but approximately 23 kcal/mol (CCSD(T)/cc-pVTZ//B3LYP/cc-pVTZ) higher in energy than pyridine [43].

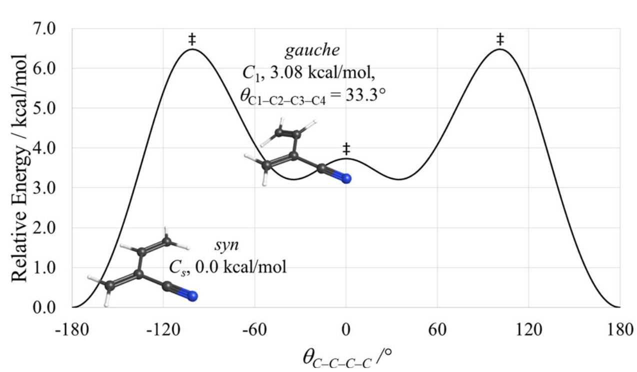

Figure 2. Computed conformational potential energy surface of 2-cyano-1,3-butadiene (B3LYP/6-311+G(2d,*p*)).

Analysis of rotational spectra

As expected – based upon the conformational analysis, the comparable dipole moments (B3LYP/6-311+(2d,p)) of the *syn* ($\mu_a = 3.2$ D, $\mu_b = 2.3$ D) and *gauche* ($\mu_a = 3.9$ D, $\mu_b = 1.6$ D, $\mu_c = 0.1$ D) conformers, and the very dense spectrum of the *syn* conformer – only the *syn* conformer (Figure 3) was observed in the spectrum. The spectral density of thousands of observable transitions for each of the three lowest-energy vibrational states in this frequency range is compounded by the fact that there are many additional vibrational states with transitions more intense than the *gauche* conformer (1080 cm^{-1}). Figure 4 shows the manifold of 16 vibrationally excited states with energies less than 500 cm^{-1}. The ground state is separated from the lowest-energy excited vibrational state, ν_{27}, by 144 cm^{-1} and was thus

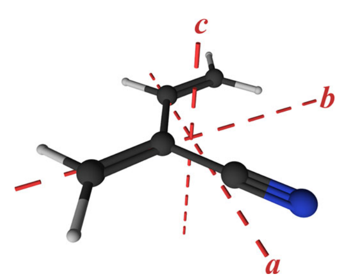

Figure 3. *syn*-2-Cyano-1,3-butadiene structure with principal inertial axes.

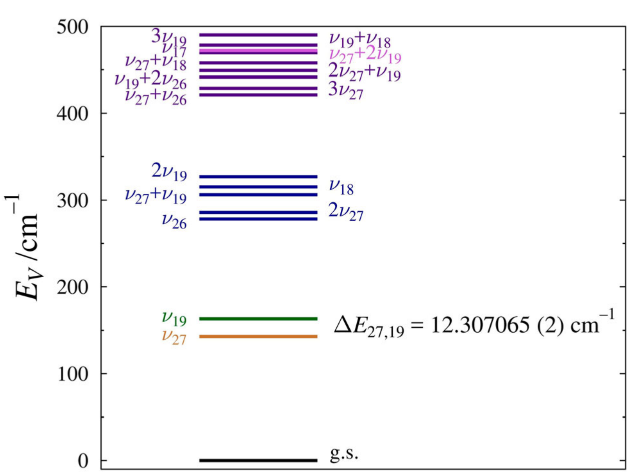

Figure 4. Vibrational energy levels of *syn*-2-cyano-1,3-butadiene below 500 cm^{-1} from computed fundamental frequencies (B3LYP/6-311+G(2d,*p*)). The value of $\Delta E_{27,19}$ results from the experimental perturbation analysis of ν_{27} and ν_{19} in this work.

expected to behave as a distorted rotor. The first two fundamentals ν_{27} (A″, 144 cm^{-1}) and ν_{19} (A′, 163 cm^{-1}) are much closer in energy (19 cm^{-1}) and were expected to require a coupled-dyad treatment. Centred around 300 cm^{-1}, there is a pentad of the first overtone states ($2\nu_{27}$ and $2\nu_{19}$), first combination state ($\nu_{27}+\nu_{19}$), and third and fourth fundamentals (ν_{26} and ν_{18}). While higher-energy vibrational states are also visible in the spectrum, the assignment and least-squares fitting of their spectra is not addressed in the current work.

Ground state

syn-2-Cyano-1,3-butadiene is a highly asymmetric oblate-top molecule (C_s, $\kappa = 0.187$) with large a-axis and b-axis dipole moments. Its rotational spectrum is dominated by clearly distinguishable R-branch bands comprised of strong, degenerate $^{a}R_{0,1}$, $^{b}R_{-1,1}$, and $^{b}R_{1,1}$ transitions. While these transitions are easily assignable in the early stages of fitting, the Q-branch transitions are much more spread out than the R-branch transitions, making the Q-branch transitions difficult to visibly discern before a fairly predictive least-squares fit is established. A portion of the experimental spectrum in the region near 167.65 GHz is provided in Figure 5, which depicts a typical R-branch series near its bandhead. We did not observe hyperfine-resolved transitions due to N-quadrupole coupling in our frequency range. Strong transitions of vibrationally excited states are also clearly visible in Figure 5, many of which can be attributed to the two lowest-energy states, ν_{27} and ν_{19}.

Transitions for the ground state of *syn*-2-cyano-1,3-butadiene were fit to a distorted-rotor Hamiltonian with octic centrifugal distortion terms (A-reduced, I^{r} representation and S-reduced, III^{r} representation). The resulting spectroscopic parameters are presented in Table 1, along with their corresponding computational values for the S-reduced, III^{r} representation. Due to the large a-axis and b-axis dipole moments, the broad spectral range, and the large number of transitions ($>$ 4000) included in the least-squares fit, all octic centrifugal distortion terms were satisfactorily determined in a fit with low statistical error (0.033 MHz). The predicted quartic and sextic centrifugal distortion constants, with the exception of d_1, are in good agreement with the experimental values. The predicted rotational constants are within 2% and all of the distortion constants agree to within 12%, with the clear exception of d_1. While it may initially seem surprising that d_1 is predicted to have the opposite sign from that determined experimentally, it is likely due to the very small magnitude of d_1 – almost 50× smaller than the next smallest quartic distortion constant. A slight underprediction of the near-zero d_1 value leads to a negative value. Although it would be highly desirable to

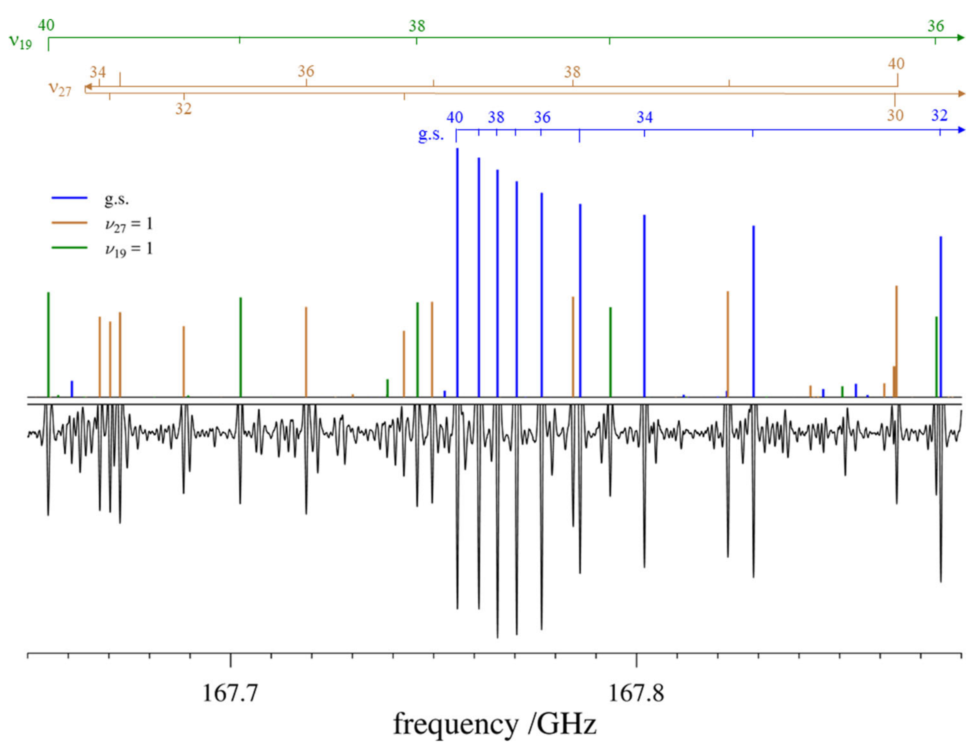

Figure 5. 2-Cyano-1,3-butadiene rotational spectrum from 167.65 to 167.88 GHz (bottom) and stick spectra for the ground vibrational state, ν_{27}, and ν_{19} of the *syn* conformer (top). Values on the numberlines at the top indicate the $J'' + 1$ values of the corresponding transitions.

Table 1. Experimental and computational spectroscopic constants for the ground vibrational state of *syn*-2-cyano-1,3-butadiene.

S Reduction, III^r representation				A Reduction, I^r representation		
	Experimental[a]		B3LYP		Experimental	
A_0 (MHz)	4773.019689	(77)	4819.	A_0 (MHz)	4773.011589	(78)
B_0 (MHz)	3665.214370	(55)	3607.	B_0 (MHz)	3665.217803	(55)
C_0 (MHz)	2071.623950	(66)	2061.	C_0 (MHz)	2071.626692	(66)
D_J (kHz)	2.883776	(44)	2.73	Δ_J (kHz)	2.506066	(32)
D_{JK} (kHz)	−5.075865	(77)	−4.73	Δ_{JK} (kHz)	−9.656771	(82)
D_K (kHz)	2.375684	(42)	2.18	Δ_K (kHz)	11.89902	(10)
d_1 (kHz)	0.020027	(25)	−0.0510	δ_J (kHz)	1.161226	(11)
d_2 (kHz)	−0.9523601	(95)	−0.923	δ_K (kHz)	−0.181326	(43)
H_J (Hz)	0.010119	(12)	0.00918	Φ_J (Hz)	0.0069441	(76)
H_{JK} (Hz)	−0.036931	(26)	−0.0331	Φ_{JK} (Hz)	−0.030943	(37)
H_{KJ} (Hz)	0.044472	(24)	0.0396	Φ_{KJ} (Hz)	0.006032	(62)
H_K (Hz)	−0.017681	(10)	−0.0157	Φ_K (Hz)	0.044383	(51)
h_1 (Hz)	0.001990	(10)	0.00192	ϕ_J (Hz)	0.0034811	(28)
h_2 (Hz)	0.0050266	(64)	0.00468	ϕ_{JK} (Hz)	−0.010379	(16)
h_3 (Hz)	0.0011408	(12)	0.00104	ϕ_K (Hz)	0.029736	(20)
L_J (μHz)	−0.0435	(12)		L_J (μHz)	−0.01135	(59)
L_{JJK} (μHz)	0.2024	(31)		L_{JJK} (μHz)	0.0542	(52)
L_{JK} (μHz)	−0.3960	(40)		L_{JK} (μHz)	−0.178	(11)
L_{KKJ} (μHz)	0.3488	(31)		L_{KKJ} (μHz)	0.504	(13)
L_K (μHz)	−0.1112	(12)		L_K (μHz)	−0.5463	(96)
l_1 (μHz)	−0.0259	(12)		l_J (μHz)	−0.00586	(24)
l_2 (μHz)	−0.0282	(10)		l_{JK} (μHz)	0.0353	(21)
l_3 (μHz)	−0.01357	(36)		l_{KJ} (μHz)	0.1162	(36)
l_4 (μHz)	−0.001241	(68)		l_K (μHz)	−0.4869	(51)
Δ_i (uÅ^2)[b]	0.185363	(8)	0.228	Δ_i (uÅ^2)[b]	0.184990	(8)
N_{lines}[c]	4185			N_{lines}[c]	4185	
σ_{fit} (MHz)	0.033			σ_{fit} (MHz)	0.033	

[a]Converted from III^l representation by applying opposite sign to all odd-numbered, off-diagonal distortion constants.
[b]Inertial defect, $\Delta_i = I_c - I_a - I_b$. Calculated using PLANM from the B_0 constants.
[c]Number of fitted transition frequencies.

compare the experimentally determined octic centrifugal distortion constants with their theoretically predicted values, current computational chemistry software packages cannot perform these calculations, because they require the implementation of higher-order vibrational perturbation theory. Data distribution plots for measured R- and Q-branch transitions are provided in Figure 6, demonstrating the breadth of data. Q-branch transitions cover a range of K_a values from 0 to 60 and J'' values from 33 to 100. R-branch transitions cover a range of K_a values from 0 to 55 and J'' values from 13 to 85.

The lowest-energy vibrationally excited states ν_{27} and ν_{19}

The two lowest-energy vibrationally excited states, ν_{27} (A$''$, 144 cm^{-1}) and ν_{19} (A$'$, 163 cm^{-1}), are an *a*-type and *b*-type Coriolis-coupled dyad. The lowest-energy vibration (ν_{27}) is a torsion about the C2–C3 bond, while ν_{19} is an in-plane wag of the cyano group. The data distribution plots for ν_{27} and ν_{19} are provided in Figure 7. The measured transitions cover a narrower range of quantum numbers than the ground state, as would be expected due to the lower intensity of the vibrationally excited states. The data distribution plots for ν_{27} and ν_{19} look similar to one another, as well as to the ground-state plot, with regard to the distribution of larger errors, indicating no obvious systematic error in the coupled-state treatment.

Both *a*- and *b*-types of Coriolis coupling have a discernable effect on the spectra of ν_{27} and ν_{19} as a result of the C_s symmetry of *syn*-2-cyano-1,3-butadiene, its large *a*- and *b*-type dipole moments, and its substantial Coriolis-coupling constants ($\zeta^a_{27,19}$ and $\zeta^b_{27,19}$). These Coriolis-coupling constants are directly related to the spectroscopic constants G_a and G_b through Eq. (1), where ω is the harmonic vibrational frequency of the corresponding mode, and x is the corresponding inertial axis [44].

$$G_x = \frac{\omega_{27} + \omega_{19}}{\sqrt{\omega_{27} \times \omega_{19}}}\, \zeta^x_{27,19} B^x_e \approx 2\zeta^x_{27,19} B^x_e \qquad (1)$$

The initial least-squares fitting of ν_{27} and ν_{19} was remarkably straightforward, using the predicted G_a and G_b values, the predicted energy difference, and the ground-state distortion constants. The values of C_v were predicted using the experimental C_0 value and the corresponding computed vibration-rotation interaction constants,

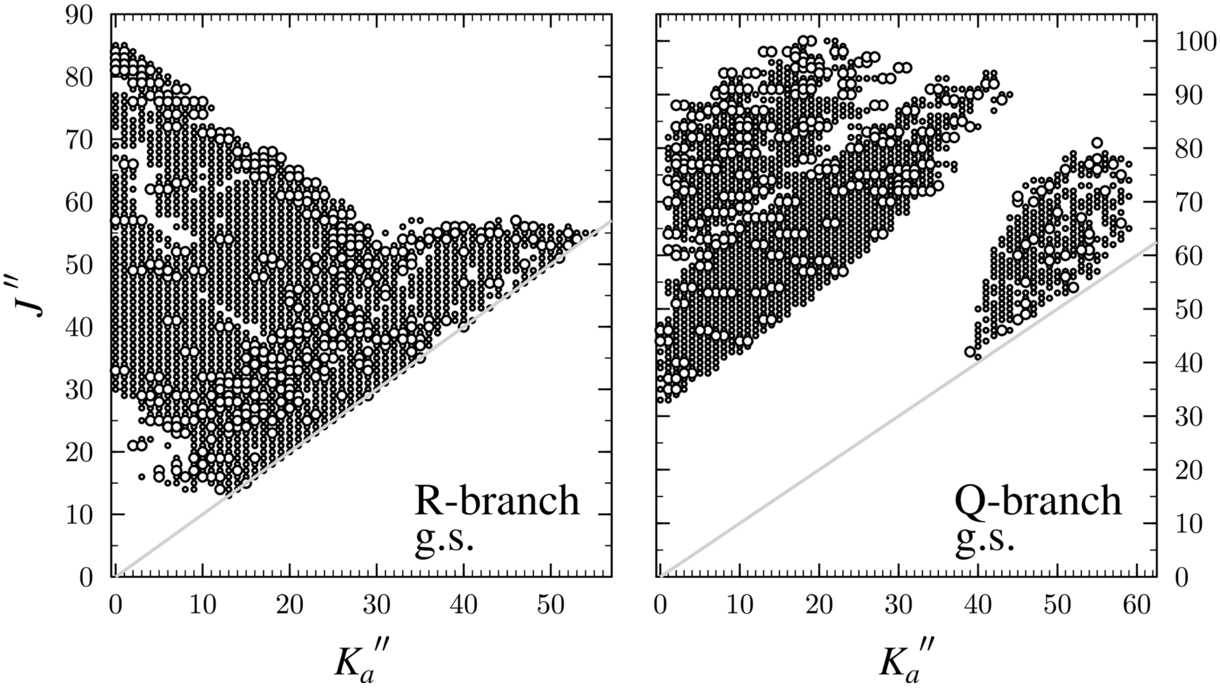

Figure 6. Data distribution plot for the least-squares fit of spectroscopic data for the vibrational ground state of *syn*-2-cyano-1,3-butadiene. The size of the plotted symbol is proportional to the value of $|(f_{\text{obs.}} - f_{\text{calc.}})/\delta f\,|$, where δf is the frequency measurement uncertainty (0.05 MHz), and all values shown are smaller than 3.

while the values of A_v and B_v were set to corresponding experimental ground-state values. As the first dozen R-branch K_a series were added to the least-squares fit, it became possible to fit G_b and the interaction between the states could be relatively well modelled. Adding higher K_a series enabled inclusion of G_a and higher-order coupling terms. Fitting of the available R- and Q-branch transitions, including resonances and nominal interstate transitions, resulted in a low-error (0.040 MHz) least-squares fit with a well-determined energy separation and several coupling coefficients. While the value of G_b and the energy separation remained relatively stable throughout the fitting process, the value of G_a was volatile. In the end, two different solutions, labelled Fit I and Fit II, were able to model the spectra with the same energy difference, $\Delta E_{27,19} = 12.307065\,(2)\ \text{cm}^{-1}$. Table 2 presents the ground-state spectroscopic constants in the A reduction, I^{r} representation, along with two sets of spectroscopic constants for the ν_{27}:ν_{19} dyad. The octic centrifugal distortion constants, not shown explicitly in the table, are held constant at their corresponding ground-state values.

Fit I and Fit II are both presented here because it is unclear which set of spectroscopic constants is more physically meaningful. Fit I and Fit II are distinguished by the inclusion (Fit I) or exclusion (Fit II) of F_{ac}^{J} in the Hamiltonian. Inclusion of this coupling term has a relatively small impact on the rotational and distortion constants, but a relatively large impact on G_a and other Coriolis coupling terms. Between the two least-squares fits, the values of the corresponding states' rotational constants differ by less than 0.01%. The quartic distortion constants agree within 0.25% between fits, with the exception of δ_K. The latter differs by 1.8% for ν_{27} and 2.5% for ν_{19} upon exclusion of F_{ac}^{J}. This difference does not, however, appear to be substantial, considering that δ_K changes by approximately 14% and 35% upon excitation from the ground state to ν_{27} and ν_{19}, respectively. Similarly, Φ_J and ϕ_J for both states change by 2.0-2.5% between the two fits, the values of Φ_{JK} are within 1.2% for both states, and the other fitted sextic distortion constants are within 0.45%. In contrast, the value of G_a in Fit I increases by 40.2% in Fit II. As might be expected, the other F_{ac} terms are also impacted substantially by inclusion or exclusion of F_{ac}^{J}. Importantly, however, the energy separation between the two least-squares fits is nearly unaffected by the inclusion or absence of F_{ac}^{J}, and the two values fall within the experimental error of one another – determined to the millionth of a wavenumber digit. The experimentally determined value (12.307065 (2) cm^{-1}) is approximately two-thirds of the predicted value (19.605 cm^{-1}).

In order to discern the better, or more physically meaningful, of the two least-squares fits, one might compare the experimentally determined values to those predicted computationally. The B3LYP prediction of G_b is 1918 MHz, which is approximately 11% different from

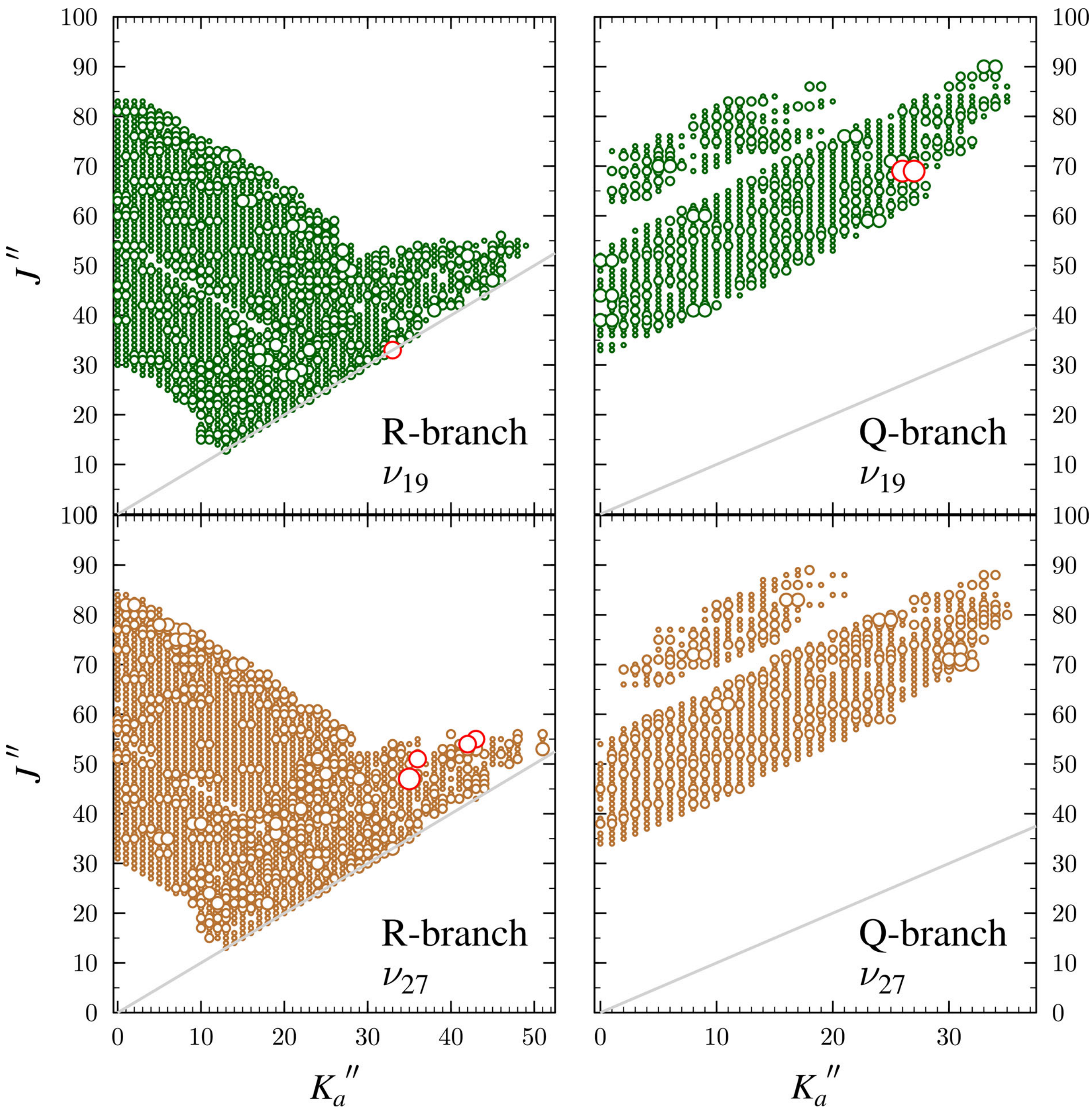

Figure 7. Data distribution plots for the coupled fit (Fit I, *vide infra*) of measured transitions in the two lowest-energy excited vibrational states in *syn*-2-cyano-1,3-butadiene. The size of the plotted symbol is proportional to the value of of $|(f_{\text{obs.}} - f_{\text{calc.}})/\delta f\,|$, where δf is the frequency measurement uncertainty (50 kHz). Values for which this relative error is > 3 are plotted in red.

1731.9 (10) MHz in Fit I and 12% different from the 1708.65 (70) MHz in Fit II. The value of G_a, however, is predicted to be 1025.44 MHz. This value is nearly an order of magnitude larger than the value determined in Fit I (135.1 (19) MHz), and the value in Fit II is only 54 MHz closer to the prediction. Since predictions of additional coupling terms – their values or even which terms are necessary to properly address coupling between perturbing states – are not readily available, computational predictions do not offer an effective way to suggest which of the two sets of constants is more physically meaningful. The two least-squares fits do agree on the energy separation between ν_{27} and ν_{19} within the error of the energy (368956.53 (5) MHz). The errors of the fits and comparison of the spectroscopic constants to their ground-state values do not provide a clear answer, either. Inclusion of an additional coupling term could affect the extent of state mixing, and therefore change the predicted intensities of various transitions. None of the observed transitions' predicted intensities, however, differ sufficiently between Fit I and Fit II to enable a choice based on transition intensities. The fact that Fit I enabled the fitting of 81 more transitions than Fit II appears to be the only indication that Fit I is better able to model

Table 2. Experimentally determined parameters for ν_{27} and ν_{19} excited vibrational states of *syn*-2-cyano-1,3-butadiene compared to those for the ground state (A-reduced Hamiltonian, I^r representation).[a]

	ground state		Fit I ν_{27} (A'', 144 cm^{-1})		Fit I ν_{19} (A', 163 cm^{-1})		Fit II ν_{27} (A'', 144 cm^{-1})		Fit II ν_{19} (A', 163 cm^{-1})	
A_v (MHz)	4773.011589	(78)	4777.0079	(15)	4791.5856	(13)	4777.0574	(17)	4791.5398	(16)
B_v (MHz)	3665.217803	(55)	3649.663	(10)	3665.811	(10)	3649.4474	(65)	3666.0288	(65)
C_v (MHz)	2071.626692	(66)	2073.14036	(11)	2069.96427	(11)	2073.137345	(69)	2069.961582	(89)
Δ_J (kHz)	2.506066	(32)	2.48463	(22)	2.45624	(22)	2.47990	(15)	2.46104	(14)
Δ_{JK} (kHz)	−9.656771	(82)	−9.67560	(49)	−9.37343	(49)	−9.66066	(15)	−9.38847	(17)
Δ_K (kHz)	11.89902	(10)	11.91046	(18)	11.77140	(19)	11.90831	(17)	11.77322	(18)
δ_J (kHz)	1.161226	(11)	1.14949	(10)	1.13712	(10)	1.147151	(73)	1.139456	(73)
δ_K (kHz)	−0.181326	(43)	−0.15618	(29)	−0.11757	(29)	−0.15896	(28)	−0.11469	(28)
Φ_J (Hz)	0.0069441	(76)	0.0070293	(80)	0.0062762	(89)	0.0068778	(65)	0.0064332	(75)
Φ_{JK} (Hz)	−0.030943	(37)	−0.031698	(21)	−0.028573	(26)	−0.031361	(20)	−0.028907	(25)
Φ_{KJ} (Hz)	0.006032	(62)	[0.006032]		[0.006032]		[0.006032]		[0.006032]	
Φ_K (Hz)	0.044383	(51)	0.045319	(64)	0.044718	(82)	0.045369	(70)	0.044513	(83)
ϕ_J (Hz)	0.0034811	(28)	0.0035287	(39)	0.0031480	(42)	0.0034552	(32)	0.0032223	(36)
ϕ_{JK} (Hz)	−0.010379	(16)	−0.010658	(11)	−0.010148	(11)	−0.010624	(12)	−0.010181	(11)
ϕ_K (Hz)	0.029736	(20)	[0.029736]		[0.029736]		[0.029736]		[0.029736]	
ΔE (MHz)			368956.534	(49)			368956.516	(50)		
ΔE (cm^{-1})			12.3070652	(16)			12.3070646	(17)		
G_a (MHz)			135.1	(19)			189.4	(16)		
G_a^J (MHz)			−0.027244	(60)			−0.026539	(64)		
G_a^K (MHz)			0.005204	(57)			0.004510	(60)		
F_{bc} (MHz)			−4.106	(24)			−3.450	(21)		
G_b (MHz)			1731.9	(10)			1708.65	(70)		
G_b^K (MHz)			0.024318	(92)			0.021749	(43)		
F_{ac} (MHz)			1.598	(14)			2.0219	(44)		
F_{ac}^J (MHz)			0.00001080	(34)			[0.0]			
F_{ac}^K (MHz)			−0.00002339	(43)			−0.00001578	(37)		
Δ_i (uÅ^2) [b]	0.184990	(8)	−0.49221	(38)	0.81366	(38)	−0.49894	(25)	0.82117	(25)
N_{lines} [c]			3039		3013		2994		2977	
σ (MHz)			0.040		0.039		0.040		0.040	

[a]Values in square brackets held fixed at the specified value in the least-squares fit.
[b]Inertial defect, $\Delta_i = I_c - I_a - I_b$. Calculated using PLANM from the B_0 constants.
[c]Number of fitted transition frequencies.

the rotational spectra of ν_{27} and ν_{19}. While there is no evident commonality between these 81 lines, a number of them are affected by resonances. Attempts to fit additional distortion constants or coupling terms resulted in either non-convergence of the least-squares fit, or constants that were not well-fit and did not meaningfully improve the least-squares fit.

Since our group has not previously encountered a case where a coupling term, such as G_a, has been so poorly predicted, we attempted to find a third least-squares fit with a G_a value closer to that predicted. It is evident that a- and b-type Coriolis coupling terms interplay with one another. We thus considered that, while it may appear reasonable to attempt to fit the zero$^{\text{th}}$-order coupling terms (*i.e.* G_a and G_b) first, followed by the higher-order terms, perhaps it is necessary to first fit one set (*e.g.* all b-type terms) before fitting the other, to prevent convolution of their effects. Fit III was attempted in this manner – by first fitting the b-type Coriolis coupling terms. At early stages and throughout the fitting process, we attempted to fit G_a in order to observe its effect. At these early stages, however, the least-squares fit failed to converge when G_a was allowed to vary, and there was nearly no effect on the overall error of the least-squares fit. This seemed to indicate both that there was not sufficient data to address G_a, and that G_a was not the most important term for addressing perturbation in low K_a series. Addition of G_b addressed the global perturbation observed in low K_a series and allowed b-type resonances to be fit, along with additional b-type coupling terms, while the a-type resonances continued to be poorly predicted. Around $K_a = 16$–20, a curvature resembling a global perturbation became evident in Loomis-Wood plots. No distortion terms were able to address this curvature and, after addition of several such series, the least-squares fit failed to converge. At this point, inclusion of G_a enabled convergence and substantially decreased the overall error of the least-squares fit. The spectral prediction using the resulting constants eliminated the curvature previously observed in Loomis-Wood plots and began to bring

a-type resonances closer to fitting. Through this procedure, however, the value of G_a dropped from 1025 to ~300 MHz. It is expected that further fitting and refinement would lead to Fits I and II, and not result in a G_a value closer to the computational prediction. To further test the sensitivity of G_a to the inclusion or omission of other, higher-order Coriolis terms, we also attempted a least-squares fit of the spectroscopic data with F_{bc} arbitrarily set to zero. The fitting procedure did converge, and in fact, the value of G_a did increase to 453 MHz. This value, however, remains far from the predicted value. Moreover, this fit was inferior to Fits I and II in several respects, including its inability to fit many resonances, and was therefore not considered further.

As it appears that Fit I better models the rotational spectra of ν_{27} and ν_{19}, all discussion henceforth refers to Fit I. In comparison to the ground state, the rotational and distortion constants of ν_{27} and ν_{19} appear to be reasonably determined, physically meaningful values. The values of the rotational constants for both vibrationally excited states are within 0.5% of the corresponding ground-state constant. Upon excitation to ν_{27}, the largest change occurs in the value of B_{27}, whereas the largest change upon excitation to ν_{19} occurs in A_{19}. Among the distortion constants, δ_K displays the largest changes from the ground state by 13.9% for ν_{27} and 35.2% for ν_{19}. Although the percent change of δ_K for ν_{19} is the largest of any of the constants, it may parallel the large change in A_{19} from the ground-state value. Since the values of δ_K for the two vibrationally excited states do not diverge from the ground-state value (shift of equal magnitude, but opposite direction), we do not expect that they are absorbing perturbation. Moreover, δ_K does not appear in the table of most strongly correlated values (correlation matrix provided in the fitting output file and in the supplemental material). All of the fitted sextic distortion constants for ν_{27} are within 3% of the corresponding ground-state values, with the values of Φ_{JK} and ϕ_{JK} having the greatest change upon excitation. Upon excitation to ν_{19}, the greatest change is observed in Φ_J and ϕ_J, which both change by approximately 9.6% from the ground state.

Interpretation and analysis of the resonances

The resonance landscape of ν_{27} and ν_{19} is dominated, both in quantity and in size, by a-type resonances, *i.e.* resonances that have an even number value of ΔK_a between the near-resonant ν_{19} and ν_{27} states. Such a-type resonances observed in ${}^{a}\mathrm{R}_{0,1}$ branch transitions in this work have perturbing interactions between opposite-symmetry states. That is, one series exhibiting resonance behaviour involves transitions with quantum numbers where $K_a + K_c = J$ (denoted with a superscript '+' over the K_a value), and the corresponding series in the other perturbing state involves transitions between levels with quantum numbers $K_a + K_c = J + 1$ (denoted with a superscript '−' over the value of K_a). An example of such a pair of resonance plots is provided in Figure 8, where the selection rule for this particular set of resonances is $\Delta K_a = 2$. This set of transitions displays one of the most substantial displacements observed in the current work, appearing approximately 6.3 GHz away from the frequency that would be expected absent the local perturbation. In general, a-type resonances within the quantum number range of the work presented here are predicted to appear up to 7.8 GHz away from their expected location without perturbation, although the transitions with the largest displacements fall just outside of the spectral range in which we can measure them. All of the a-type resonances we observed conform to a $\Delta K_a = 2$ or 4 selection rule. The b-type resonances ($\Delta K_a =$ odd number selection rule) in our spectral region tend to exhibit smaller displacements than the a-type resonances. An example is depicted in Figure 9, where $\Delta K_a = 5$ and the maximum local perturbation is less than 0.5 GHz from the expected location absent local perturbation. Unlike the a-type resonances, perturbing states involved in b-type resonances have the same symmetry.

The Coriolis coefficient G_b is much larger than G_a, while the a-type resonances dominate the observed spectral region both in quantity and magnitude. A set of resonance progression plots, presented in Figure 10, display both a set of ${}^{a}\mathrm{R}_{0,1}$ branch, K_a series and a set of ${}^{b}\mathrm{R}_{1,1}$ branch, K_a series (even values of K_a only). In these plots, the y-axis displays the difference between the ν_{27} transition frequency and its corresponding 'deperturbed' transition frequency, scaled by $J''+1$. The deperturbed frequency is that predicted using the same spectroscopic constants as in the coupled-state fit, but excluding all coupling terms, enabling a visualisation of the effect of the Coriolis coupling. Patterns observed in other Coriolis-coupled states of planar molecules [1,45–49], such as the presence and progression of a global undulation and an increase in resonance magnitude with increasing J, appear in these plots, as well.

For *syn*-2-cyano-1,3-butadiene, the resonance plots for the a-type, R-branch transitions (Figure 10, top panel) and for the b-type, R-branch transitions (Figure 10, bottom panel) are identical at higher values of $J''+1$. The prominent resonances occur in that high-J region, where the a- and b-type transitions are degenerate. At lower values of $J''+1$, however, the a- and b-type transitions are non-degenerate, and the global perturbation behaviour observed differs significantly between the two sets of

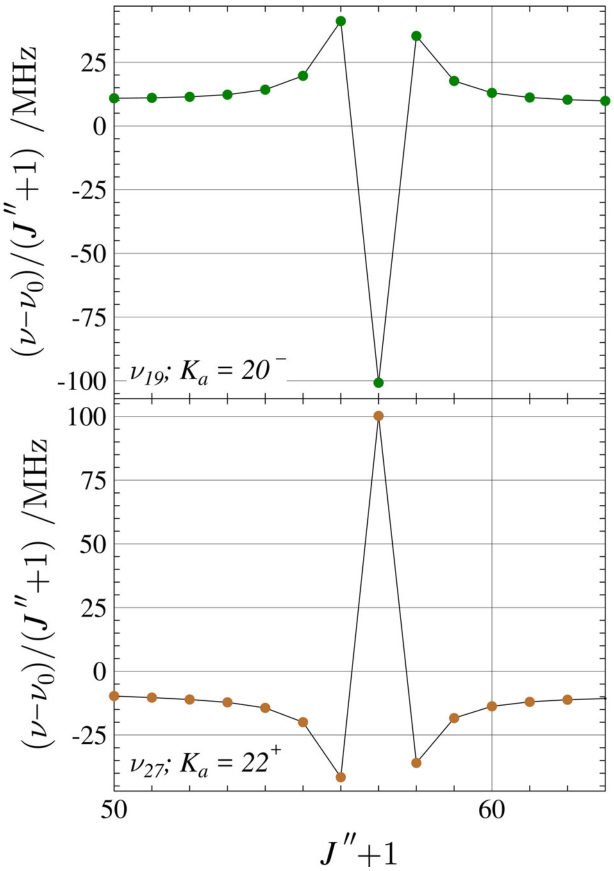

Figure 8. Resonance plots for *syn*-2-cyano-1,3-butadiene showing the $K_a = 22^+$ series for ν_{27} and $K_a = 20^-$ series for ν_{19}, an example of resonances conforming to the $\Delta K_a = 2$ selection rule. The plotted values are frequency differences between excited-state transitions and their ground-state counterparts, scaled by $(J''+1)$ in order to make the plots more horizontal. Measured transitions are represented by circles: ν_{27} (copper), ν_{19} (green). There are no measured transitions with $|(f_{obs.}-f_{calc.})/\delta f\,| > 3$. Predictions from the final coupled fit are represented by a solid, black line. The two resonances are mirror images of one another, confirming the K_a assignment of these resonance partners.

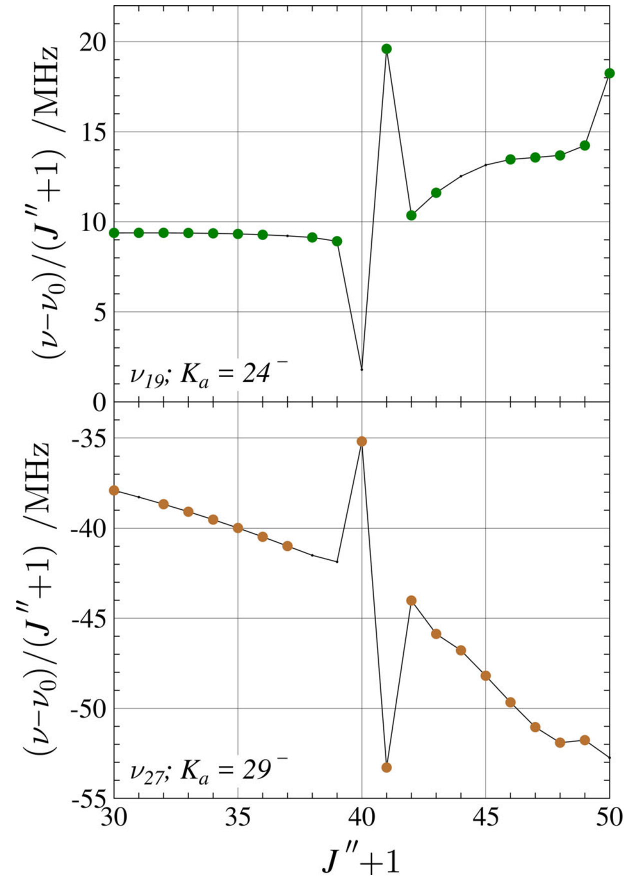

Figure 9. Resonance plots for *syn*-2-cyano-1,3-butadiene showing the $K_a = 29^-$ series for ν_{27} and $K_a = 24^-$ series for ν_{19}, an example of resonances conforming to the $\Delta K_a = 5$ selection rule. The plotted values are frequency differences between excited-state transitions and their ground-state counterparts, scaled by $(J''+1)$ in order to make the plots more horizontal. Measured transitions are represented by circles: ν_{27} (copper), ν_{19} (green). The missing data point at $J''+1 = 40$ in the plot of ν_{19} was not included, due to overlap with a ground-state transition. There are no measured transitions with $|(f_{obs.}-f_{calc.})/\delta f\,| > 3$. Predictions from the final coupled fit are represented by a solid, black line. The features of the two resonance plots are mirror images of one another, confirming the K_a assignment of these resonance partners.

transition types. While the undulation in the *a*-type plot has a serpentine shape whose amplitude increases only slightly with increasing K_a (Figure 10, top panel), the shape of the undulation in the *b*-type plot is akin to a hill shape whose amplitude increases more rapidly (Figure 10, bottom panel).

Figure 11 shows the same ${}^{b}\mathrm{R}_{1,1}$ resonance progression plot for *syn*-2-cyano-1,3-butadiene as in Figure 10, but over a smaller set of $J''+1$ values and such that each K_a series is vertically staggered to better elucidate the shape of resonances. The large resonances in K_a series 6 through 16 are somewhat inconsistent in shape and do not increase in position by a steady value of *J*, indicating that the energy-level crossings responsible for these resonances occur at variable intervals between *J* values. After $K_a = 16$, the resonances of the ν_{27}:ν_{19} dyad of *syn*-2-cyano-1,3-butadiene take on a more regular shape and *J* progresses in regular steps of three.

As part of the coupled-state analysis, 16 matched pairs of nominal interstate transitions are included in Fit I. The formally forbidden, simultaneous vibrational and rotational transitions are enabled by substantial energy-level mixing between the two states. An example of a matched pair is depicted in Figure 12. In order for a pair of nominal interstate transitions to be a matched pair, their quantum numbers must describe two real, within-state transitions when either the upper or the lower energy levels are swapped between the nominal interstate transitions.

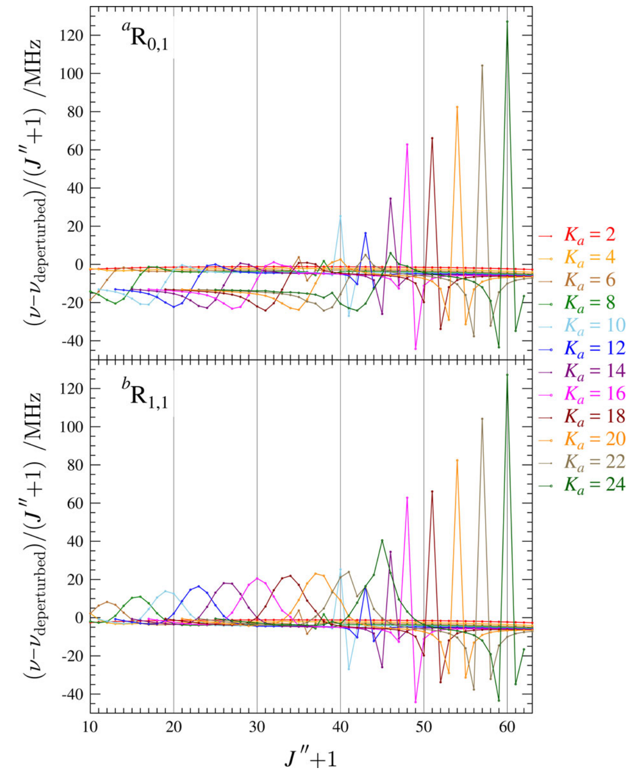

Figure 10. Superimposed resonance plots of ν_{27} for ^{a}R$_{0,1}$ K_a^+ (top) and ^{b}R$_{1,1}$ (bottom) series with even values of K_a between 2 and 24 for *syn*-2-cyano-1,3-butadiene. Measured transitions are omitted for clarity, but they are indistinguishable from the plotted values on this scale. The plotted values are frequency differences between excited-state transitions and their deperturbed counterparts, scaled by ($J''+1$). The *x*- and *y*-axes are set to the same scale for each of the resonance plots.

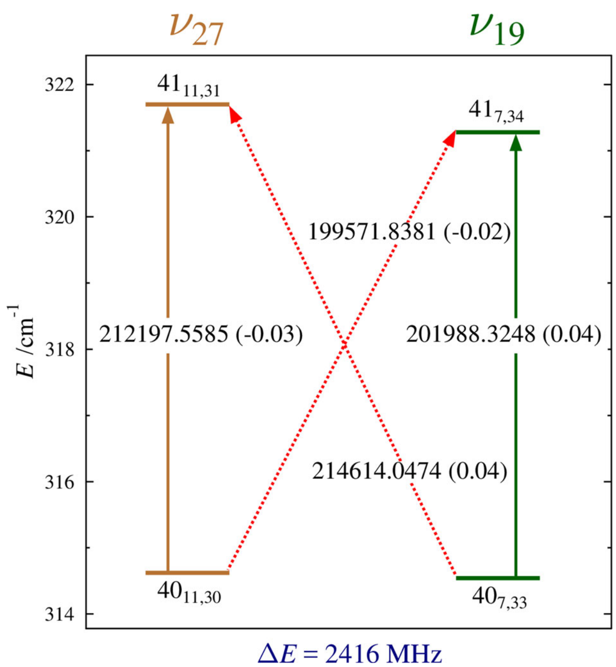

Figure 12. Energy diagram depicting a representative matched pair of nominal rotation-vibration transitions between ν_{27} (copper) and ν_{19} (green) vibrational states of *syn*-2-cyano-1,3-butadiene. Standard ^{a}R$_{0,1}$ transitions within vibrational states are denoted by vertical arrows. The diagonal, dashed arrows indicate nominal interstate transitions that are formally forbidden, but enabled as a result of vibrational-rotational state mixing. Values printed on each of the arrows are the corresponding transition frequency (in MHz) with its *obs.* – *calc.* value in parentheses. The marked energy separation is the energy separation between the two strongly interacting rotational energy levels.

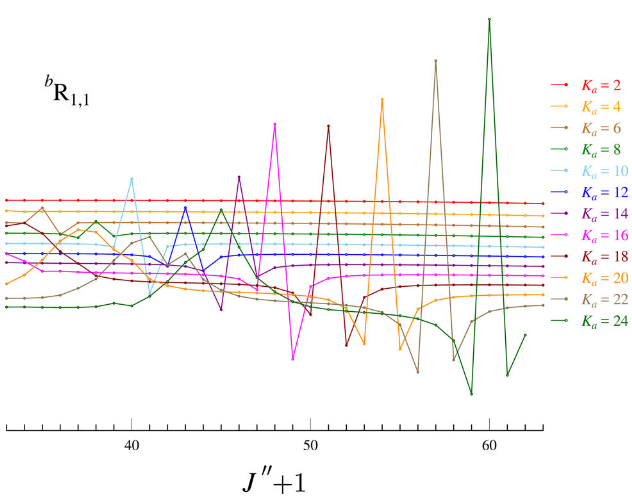

Figure 11. Superimposed resonance plots of ν_{27} for ^{b}R$_{1,1}$ series with even values of K_a between 2 and 24 for *syn*-2-cyano-1,3-butadiene, vertically offset to simplify viewing individual plots. Measured transitions are omitted for clarity, but they are indistinguishable from the plotted values on this scale. The plotted values are frequency differences between excited state transitions and their deperturbed counterparts, scaled by ($J''+1$).

Matched pairs of nominal interstate transitions, therefore, have the same J values and their frequencies are typically predicted equally well. The average frequency of the within-state transitions and the average frequency of the matched nominal interstate transitions must be the same, within experimental error. In the example presented in Figure 12, these averages are 0.001 MHz apart, well within the experimental error of frequency measurement. A list of the measured nominal interstate transitions along with their average frequency analysis is provided in the supplemental material.

Comparison with computational estimates

The successful analysis of perturbed vibrationally excited states is reliant upon the ability to identify and assign their transitions in an initial fit. To this end, computational predictions of the vibration-rotation interaction constants are of particular utility. A comparison of the predicted and experimental vibration-rotation interaction constants is provided in Table 3. As expected, the C_0–C_v values are quite well predicted, with the value for

Table 3. Vibration-rotation interaction constants for ν_{27} and ν_{19} of *syn*-2-cyano-1,3-butadiene.

	Experimental	B3LYP/6-311+(2*d*,*p*)
	ν_{27}	
A_0–A_{27} (MHz)	−4.00	−6.51
B_0–B_{27} (MHz)	15.55	14.36
C_0–C_{27} (MHz)	−1.51	−1.39
	ν_{19}	
A_0–A_{19} (MHz)	−18.57	−15.34
B_0–B_{19} (MHz)	−0.59	−0.86
C_0–C_{19} (MHz)	1.66	1.68
	average	
$(A_0$–$A_v)_{ave}$ (MHz)	−11.29	−10.92
$(B_0$–$B_v)_{ave}$ (MHz)	7.84	6.75
$(C_0$–$C_v)_{ave}$ (MHz)	0.075	0.14

ν_{19} remarkably close to its experimental value. The theoretical A_0–A_v and B_0–B_v values are also in generally good agreement with the experimentally determined values. For ν_{27}, the largest discrepancy is in the value of A_0–A_v, which is over-predicted by half its experimental value. For ν_{19}, it is the B_0–B_v value whose magnitude is too large by a little over one-third of the experimental value. When, however, the average of the vibration-rotation interaction constants is examined (to balance out any potentially unaddressed perturbation factors in the theoretical treatment), the A_0–A_v and B_0–B_v averages fall within 10% of their experimental counterparts.

Discussion

The coupled-state analysis presented here provides an example of a Coriolis-coupled dyad, adding to the small body of data available on such dyads involving both *a*- and *b*-type Coriolis coupling. While most of the computational predictions for both the ground and vibrationally excited states are in good agreement with the experimental data, the present dyad analysis produces a value of G_a that is in poor agreement with the theoretical prediction. This discrepancy is unexpected, given the many previously studied coupled states (particularly those containing an aromatic ring and those of propionitrile) [21,45,46,48–50], where G_a was quite well computationally predicted. Our efforts to reduce this disagreement by modifying the least-squares fit have been unsuccessful. This turns out, however, to not be the first such example [41], as one of the predicted Coriolis-coupling coefficients for ν_{14}:ν_{20} dyad of SSC-glycolic acid ($G_a^{14,20}$ = 2599.36 MHz, B3LYP/6-311+G(2d,p)) is significantly different (76%) from the corresponding experimentally determined value (1477 (22) MHz). The predicted value of $G_b^{14,20}$ (2382.82 MHz), on the other hand, is only 8% different from the experimentally determined value of 2585.0 (95) MHz. It appears, based on the limited data available, that while the Coriolis-coupling coefficients (G_x) for substituted cyclic species are predicted quite well, computing those for acyclic species accurately is not always so straightforward. Attributing this problem to inaccuracies in the calculation of the Coriolis zeta constant is difficult to justify, because this parameter only depends on the normal coordinate analysis (the structure and harmonic force field), and computed results are not at all sensitive to basis set and correlation treatment. As discussed earlier, omitting the F_{bc} term does not fully address the discrepancy between the predicted and experimental values of G_a. Perhaps the omission of some higher-order (anharmonic) term in the spectroscopic Hamiltonian is responsible for the problem, but we have not been able to identify that term so far. It is alternatively possible that the issue arises from the determination of G_a and G_b from the spectral data, as the two terms interact strongly in the observed resonances, making the accuracy of the smaller constants highly affected by any errors in the larger constant.

The ground-state rotational spectrum of *syn*-2-cyano-1,3-butadiene has been measured and analysed here for the first time, resulting in a set of spectroscopic constants that include all of the octic centrifugal distortion constants. The experimental data provide the basis for an astronomical search for this highly polar species in the interstellar medium using high-frequency data (a low-frequency search would additionally require values of the N-quadrupole coupling terms, which can be reasonably well predicted theoretically). In terms of astrochemistry, this molecule represents a significant target for detection in its own right and because it is an isomer of the long-sought heterocyclic aromatic molecule, pyridine.

Supplemental material

See supplemental material for least-squares fitting files of 2-cyano-1,3-butadiene, output files from computations, computed vibration-rotation interaction constants, computed vibrational frequencies and infrared intensities, and nominal interstate transitions for the ν_{27} and ν_{19} dyad with their corresponding within-state transitions. These files may be found at https://doi.org/10.1080/00268976.2021.1964629.

Disclosure statement

No potential conflict of interest was reported by the author(s).

Funding

This work was supported by the National Science Foundation under Grants CHE-1954270 and CHE-1664912. We thank Michael McCarthy for the loan of an Amplification-Multiplication Chain and the Harvey Spangler Award (to B.J.E.) for the funding that supported the purchase of the corresponding Virginia Diodes Zero-Bias Detector (WR5.1ZBD 140 – 220 GHz). Current and former members of our research team thank Prof. John Stanton for his friendship and for sharing scientific insights through collaborative research over many, many years.

ORCID

Maria A. Zdanovskaia http://orcid.org/0000-0001-5167-8573
Brian J. Esselman http://orcid.org/0000-0002-9385-8078
Samuel M. Kougias http://orcid.org/0000-0002-9877-0817
Aatmik R. Patel http://orcid.org/0000-0001-8835-0870
R. Claude Woods http://orcid.org/0000-0003-0865-4693
Robert J. McMahon http://orcid.org/0000-0003-1377-5107

References

[1] C.P. Endres, S. Schlemmer, P. Schilke, J. Stutzki and H.S.P. Müller. J. Mol. Spectrosc. **327**, 95 (2016). doi:10.1016/j.jms.2016.03.005
[2] H.S.P. Müller, F. Schlöder, J. Stutzki and G. Winnewisser. J. Mol. Struct. **742**, 215 (2005). doi:10.1016/j.molstruc.2005.01.027
[3] B.A. McGuire, A.M. Burkhardt, S.V. Kalenskii, C.N. Shingledecker, A.J. Remijan, E. Herbst and M.C. McCarthy. Science. **359**, 202 (2018). doi:10.1126/science.aao4890
[4] B.A. McGuire, R.A. Loomis, A.M. Burkhardt, K.L.K. Lee, C.N. Shingledecker, S.B. Charnley, I.R. Cooke, M.A. Cordiner, E. Herbst, S. Kalenskii, M.A. Siebert, E.R. Willis, C. Xue, A.J. Remijan and M.C. McCarthy. Science. **371**, 1265 (2021). doi:10.1126/science.abb7535
[5] S. Zeng, D. Quénard, I. Jiménez-Serra, J. Martín-Pintado, V.M. Rivilla, L. Testi and R. Martín-Doménech. Mon. Not. R. Astron. Soc.: Letters. **484**, L43 (2019). doi:10.1093/mnrasl/slz002
[6] J. Cernicharo, M. Agúndez, L. Velilla Prieto, M. Guélin, J.R. Pardo, C. Kahane, C. Marka, C. Kramer, S. Navarro, G. Quintana-Lacaci, J.P. Fonfría, N. Marcelino, B. Tercero, E. Moreno, S. Massalkhi, M. Santander-García, M.C. McCarthy, C.A. Gottlieb and J.L. Alonso. Astron. Astrophys. **606**, L5 (2017). doi:10.1051/0004-6361/201731672
[7] L.W. Avery, N.W. Broten, J.M. MacLeod, T. Oka and H.W. Kroto. Astrophys J, Lett. **205**, L173 (1976). doi:10.1086/182117
[8] N.W. Broten, T. Oka, L.W. Avery, J.M. MacLeod, and H.W. Kroto, Astrophys. J. Lett. **223** L105 (1978). doi:10.1086/182739
[9] H.W. Kroto, C. Kirby, D.R.M. Walton, L.W. Avery, N.W. Broten, J.M. MacLeod and T. Oka. Astrophys. J. **219**, L133 (1978). doi:10.1086/182623
[10] L.E. Snyder and D. Buhl. Astrophys. J. **163**, L47 (1971). doi:10.1086/180664
[11] C.M. Walmsley, G. Winnewisser and F. Toelle. Astron. Astrophys. **81**, 245 (1980).
[12] R.A. Loomis, A.M. Burkhardt, C.N. Shingledecker, S.B. Charnley, M.A. Cordiner, E. Herbst, S. Kalenskii, K.L.K. Lee, E.R. Willis, C. Xue, A.J. Remijan, M.C. McCarthy and B.A. McGuire. Nat. Astron. **5**, 188 (2021). doi:10.1038/s41550-020-01261-4
[13] N.W. Broten, J.M. MacLeod, L.W. Avery, W.M. Irvine, B. Hoeglund, P. Friberg and A. Hjalmarson. Astrophys. J. **276**, L25 (1984). doi:10.1086/184181
[14] F.F. Gardner and G. Winnewisser. Astrophys. J. **195**, L127 (1975). doi:10.1086/181726
[15] L.E. Snyder, J.M. Hollis, P.R. Jewell, F.J. Lovas and A. Remijan. Astrophys. J. **647**, 412 (2006). doi:10.1086/505323
[16] F.J. Lovas, A.J. Remijan, J.M. Hollis, P.R. Jewell and L.E. Snyder. Astrophys. J. Lett. **637**, L37 (2006). doi:10.1086/500431
[17] P.M. Solomon, K.B. Jefferts, A.A. Penzias and R.W. Wilson. Astrophys. J. **168**, L107 (1971). doi:10.1086/180794
[18] A. Belloche, R.T. Garrod, H.S.P. Müller and K.M. Menten. Science. **345**, 1584 (2014). doi:10.1126/science.1256678
[19] A. Belloche, R.T. Garrod, H.S.P. Müller, K.M. Menten, C. Comito and P. Schilke Astron. Astrophys. **499**, 215 (2009). doi:10.1051/0004-6361/200811550
[20] R.J. Halter, R.L. Fimmen, R.J. McMahon, S.A. Peebles, R.L. Kuczkowski and J.F. Stanton. J. Am. Chem. Soc. **123**, 12353 (2001). doi:10.1021/ja011195t
[21] M.A. Zdanovskaia, B.J. Esselman, R.C. Woods and R.J. McMahon. J. Chem. Phys. **151**, 024301 (2019). doi:10.1063/1.5100805
[22] S.M. Kougias, S.N. Knezz, A.N. Owen, R.A. Sanchez, G.E. Hyland, D.J. Lee, A.R. Patel, B.J. Esselman, R.C. Woods and R.J. McMahon. J. Org. Chem. **85**, 5787 (2020). doi:10.1021/acs.joc.9b03388
[23] M.A. Zdanovskaia, P.M. Dorman, V.L. Orr, A.N. Owen, S.M. Kougias, B.J. Esselman, R.C. Woods and R.J. McMahon. J. Am. Chem. Soc. **143**, 9551 (2021). doi:10.1021/jacs.1c03777
[24] M.C. McCarthy, K.L.K. Lee, P.B. Carroll, J.P. Porterfield, P.B. Changala, J.H. Thorpe and J.F. Stanton. J. Phys. Chem. A. **124**, 5170 (2020). doi:10.1021/acs.jpca.0c02919
[25] P. Mishra, S.M. Fritz, S. Herbers, A.M. Mebel, and T.S. Zwier. PCCP **23** 6462 (2021). doi:10.1039/D1CP00104C
[26] J.P. Ferris and J.C. Guillemin. J. Org. Chem. **55**, 5601 (1990). doi:10.1021/jo00308a017
[27] A. Jamal and A.M. Mebel. J. Phys. Chem. A. **117**, 741 (2013). doi:10.1021/jp3091045
[28] D.S.N. Parker and R.I. Kaiser. Chem. Soc. Rev. **46**, 452 (2017). doi:10.1039/C6CS00714G
[29] N. Raffaelli, in *Origins of Life: The Primal Self-Organiza tion*, edited by Richard Egel, Dirk-Henner Lankenau, and Armen Y. Mulkidjanian (Springer-Verlag, Heidelberg, 2011), Chap. 9, pp. 191.
[30] S. Pizzarello, Y. Huang and M. Fuller. Geochim. Cosmochim. Acta. **68**, 4963 (2004). doi:10.1016/j.gca.2004.05.024
[31] S. Pizzarello and Y. Huang. Geochim. Cosmochim. Acta. **69**, 599 (2005). doi:10.1016/j.gca.2004.07.031
[32] B.M. McMurtry, A.M. Turner, S.E.J. Saito and R.I. Kaiser. Chem. Phys. **472**, 173 (2016). doi:10.1016/j.chemphys.2016.03.010
[33] S.B. Charnley, Y.-J. Kuan, H.-C. Huang, O. Botta, H.M. Butner, N. Cox, D. Despois, P. Ehrenfreund, Z. Kisiel,

Y.-Y. Lee, A.J. Markwick, Z. Peeters and S.D. Rodgers. Adv. Space Res. **36**, 137 (2005). doi:10.1016/j.asr.2005.09.005

[34] B.J. Esselman, B.K. Amberger, J.D. Shutter, M.A. Daane, J.F. Stanton, R.C. Woods and R.J. McMahon. J. Chem. Phys. **139**, 224304 (2013). doi:10.1063/1.4832899

[35] Z. Kisiel, L. Pszczółkowski, I.R. Medvedev, M. Winnewisser, F.C. De Lucia and E. Herbst. J. Mol. Spectrosc. **233**, 231 (2005). doi:10.1016/j.jms.2005.07.006

[36] Z. Kisiel, L. Pszczółkowski, B.J. Drouin, C.S. Brauer, S. Yu, J.C. Pearson, I.R. Medvedev, S. Fortman and C. Neese. J. Mol. Spectrosc. **280**, 134 (2012). doi:10.1016/j.jms.2012.06.013

[37] H.M. Pickett. J. Mol. Spectrosc. **148**, 371 (1991). doi:10.1016/0022-2852(91)90393-O

[38] Z. Kisiel, in *Spectroscopy from Space*, edited by J. Demaison, K. Sarka, E.A. Cohen (Kluwer Academic Publishers, Dordrecht, 2001), pp. 91–106. < http://www.ifpan.edu.pl/ kisiel/prospe.htm > .

[39] M.J. Frisch, G.W. Trucks, H.B. Schlegel, G.E. Scuseria, M.A. Robb, J.R. Cheeseman, G. Scalmani, V. Barone, G.A. Petersson, H. Nakatsuji, X. Li, M. Caricato, A.V. Marenich, J. Bloino, B.G. Janesko, R. Gomperts, B. Mennucci, H.P. Hratchian, J.V. Ortiz, A.F. Izmaylov, J.L. Sonnenberg, D. Williams-Young, F. Ding, F. Lipparini, F. Egidi, J. Goings, B. Peng, A. Petrone, T. Henderson, D. Ranasinghe, V.G. Zakrzewski, J. Gao, N. Rega, G. Zheng, W. Liang, M. Hada, M. Ehara, K. Toyota, R. Fukuda, J. Hasegawa, M. Ishida, T. Nakajima, Y. Honda, O. Kitao, H. Nakai, T. Vreven, K. Throssell, J.A. Jr. Montgomery, J.E. Peralta, F. Ogliaro, M.J. Bearpark, J.J. Heyd, E.N. Brothers, K.N. Kudin, V.N. Staroverov, T.A. Keith, R. Kobayashi, J. Normand, K. Raghavachari, A.P. Rendell, J.C. Burant, S.S. Iyengar, J. Tomasi, M. Cossi, J.M. Millam, M. Klene, C. Adamo, R. Cammi, J.W. Ochterski,R.L. Martin, K. Morokuma, O. Farkas, J.B. Foresman and D.J. Fox, *Gaussian 16 rev C.01* (Gaussian, Inc., Wallingford, CT, 2016).

[40] J.R. Schmidt and W.F. Polik, WebMO Enterprise, version 19.0; WebMO LLC: Madison, WI, USA, 2019; http://www.webmo.net (accessed August, 2019).

[41] Z. Kisiel, L. Pszczółkowski, E. Białkowska-Jaworska and S.B. Charnley. J. Mol. Spectrosc. **321**, 13 (2016). doi:10.1016/j.jms.2016.01.014

[42] J.H. Baraban, M.-A. Martin-Drumel, P.B. Changala, S. Eibenberger, M. Nava, D. Patterson, J.F. Stanton, G.B. Ellison and M.C. McCarthy. Angew. Chem. Int. Ed. **57**, 1821 (2018). doi:10.1002/anie.201709966

[43] B.J. Sun, C.H. Huang, S.Y. Chen, S.H. Chen, R.I. Kaiser and A.H.H. Chang. J. Phys. Chem. A. **118**, 7715 (2014). doi:10.1021/jp5056864

[44] D. Papoušek and M.R. Aliev, *Molecular Vibrational-Rotational Spectra* (Elsevier Scientific Publishing Company, Prague, 1982), **Vol. 17**, p. 323.

[45] P.M. Dorman, B.J. Esselman, J.E. Park, R.C. Woods and R.J. McMahon. J. Mol. Spectrosc. **369**, 111274 (2020). doi:10.1016/j.jms.2020.111274

[46] M.A. Zdanovskaia, B.J. Esselman, H.S. Lau, D.M. Bates, R.C. Woods, R.J. McMahon and Z. Kisiel. J. Mol. Spectrosc. **351**, 39 (2018). doi:10.1016/j.jms.2018.06.004

[47] O. Pirali, Z. Kisiel, M. Goubet, S. Gruet, M.A. Martin-Drumel, A. Cuisset, F. Hindle and G. Mouret. J. Chem. Phys. **142**, 104310 (2015). doi:10.1063/1.4913750

[48] Z. Kisiel and A. Kraśnicki. J. Mol. Spectrosc. **262**, 82 (2010). doi:10.1016/j.jms.2010.05.007

[49] Z. Kisiel, E. Białkowska-Jaworska and L. Pszczółkowski. J. Mol. Spectrosc. **232**, 47 (2005). doi:10.1016/j.jms.2005.02.006

[50] Z. Kisiel, C.A. Nixon, M.A. Cordiner, A.E. Thelen and S.B. Charnley. J. Mol. Spectrosc. **372**, 111324 (2020). doi:10.1016/j.jms.2020.111324